

We are IntechOpen, the world's leading publisher of Open Access books Built by scientists, for scientists

6,900

Open access books available

186,000

International authors and editors

200M

Downloads

Our authors are among the

154

Countries delivered to

TOP 1%

most cited scientists

12.2%

Contributors from top 500 universities



WEB OF SCIENCE™

Selection of our books indexed in the Book Citation Index
in Web of Science™ Core Collection (BKCI)

Interested in publishing with us?
Contact book.department@intechopen.com

Numbers displayed above are based on latest data collected.
For more information visit www.intechopen.com



Properties and Catalytic Effects of Nanoparticles Synthesized by Levitational Gas Condensation

Young Rang Uhm

Additional information is available at the end of the chapter

<http://dx.doi.org/10.5772/intechopen.72158>

Abstract

One of the gas-phased methods of the levitational gas condensation (LGC) process was developed to obtain nanopowders with high purity. The instrument designed by unique concept using magnetically levitated melted droplet of metal is easily operated to synthesize nanopowder with highly defected surface. The complex compounds are also easily prepared using micron powder feeding (MPF) system in the instrument. The metals, ceramics, and carbon-coated metal nanoparticles prepared using the LGC are introduced in this chapter. Various applications such as magnetic and catalytic properties are also introduced. Nanoparticles prepared using LGC showed significantly enhanced catalytic activities during chemical reaction due to the high level of defects on their surface structure. The new heterogeneous catalysts of the solid nanoparticles were introduced in this chapter.

Keywords: levitational gas condensation (LGC), catalytic activities, metals and metal oxide nanoparticles, carbon encapsulated nanoparticles

1. Introduction

Among the various methods for preparing nanopowders, almost all of the processes face important challenges, such as poor control of size distribution, surface contamination, the agglomeration of the particles, and so on [1–5]. Many attempts have been made to develop processes and techniques that can synthesize nanoparticles with specific functional properties [4–6]. Dry methods such as the levitational gas condensation (LGC) process have been developed to obtain high-purity nanopowders while suppressing the agglomeration of the produced particles [7–15]. The catalytic effects of nanopowders are influenced not only by the reduced size of the particles but also by their increased surface area [16, 17]. The surface of metal oxides

exhibits nonstoichiometry, resulting from oxygen defect structures [17]. Particles prepared by the LGC process show enhanced catalytic activities due to the high level of defects on their surface structure. In this chapter, the synthesis processes and resulting properties of various nanoparticles prepared by LGC are introduced. The sections are focused on three aspects:

1. Levitational gas condensation (LGC): The unique instrument used for the synthesis of the nanoparticles is introduced in this section [18–20].
2. Magnetic metal and carbon-encapsulated metal nanoparticles: The produced magnetic metal (Ni and Fe) and carbon-encapsulated metal (Ni@C and Fe@C) nanoparticles showed a noncollinear magnetic structure between the core and surface layer of the particles. The morphologies and the dispersion stability kinetics in the solvents are introduced. Also, the carbon-encapsulated metal nanoparticles were successfully applied as a catalyst for the multicomponent Biginelli reaction [7, 9, 12, 18–23].
3. Nonmagnetic metal and metal oxides: Cu oxides, Bi, and NiO nanopowders prepared by LGC are introduced. Cu oxide and NiO alloy nanopowders are widely applied as heterogeneous catalysts in oxidizing processes used in organic synthesis. Nanopowders of bismuth (Bi) with its low melting temperature were applied as a sensor electrode for detecting heavy metals in water [9, 14, 17, 24, 25].

2. Levitational gas condensation (LGC)

The LGC method is a kind of gas-phased method in which an electric current is flowed to two inductor coils, which are each wound opposite directions. The electric current following in different direction in each coil induces a magnetic field and creates a magnetic moment, which opposes gravity on the inside lower part of the coil [11, 18]. To synthesize a nanopowder, a melted metal is continuously evaporated and condensed in the levitated condition, suspended in the magnetic field. This method is shown in **Figure 1(a)**. In this study, we modified the inductor with a downward spiral type of coil, so that the levitation region produced by the magnetic field would be more stable for the melted droplet by generating an equivalent magnetic flux density, as shown in **Figure 1(b)**.

The total LGC system is illustrated in **Figure 2**. The nanoparticles formed at the surface of the liquid droplet are then flowed to a filter by the gas stream using a vacuum pump:

2.1. Levitational gas condensation (LGC) starting materials with a melting temperature of over 900°C

Metallic atoms were evaporated from an overheated surface and condensed by cold inert gas and then collected from the filter. To stabilize the powder surface and prohibit oxidation, the powders were passivated with thin oxide layers. The LGC apparatus consists of a high-frequency induction generator, levitation and evaporation chamber, and oxygen concentration control unit.

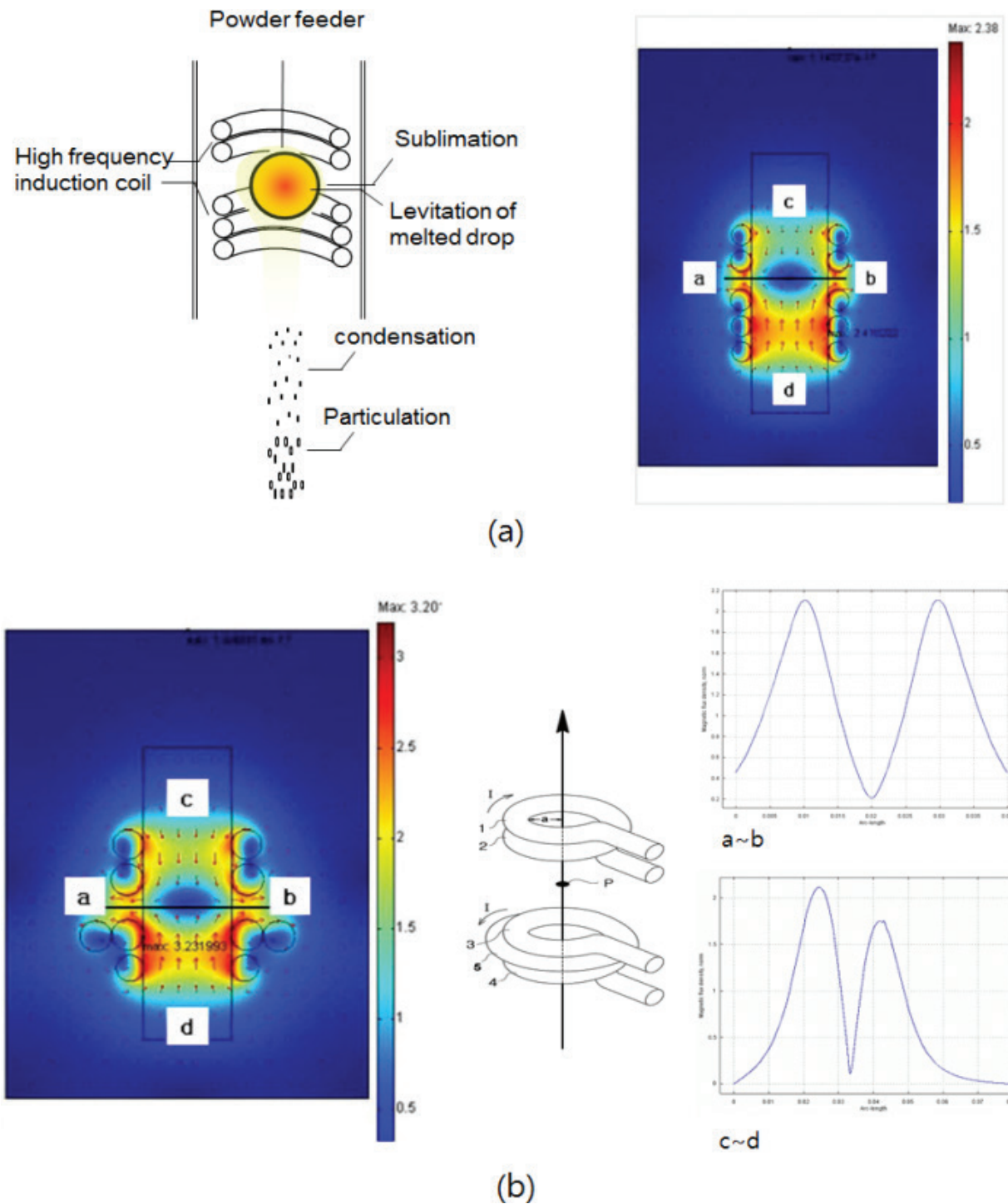


Figure 1. (a) The mechanism of forming nanoparticles and the contour maps of magnetic flux density depending on shape of inductors for a cylinder type and (b) a spiral type and its strength at in-plane (a~b) and vertical (c~d) direction [11].

The operating values used for the induction generator were 6, 5, 4.5, and 3 kW for the Ni, Fe, Cu, and Ag, respectively [7–15]. These values depended on the melting temperature as well as the magnetic permeability of the metals. The melting temperature of iron (1535°C) is higher than

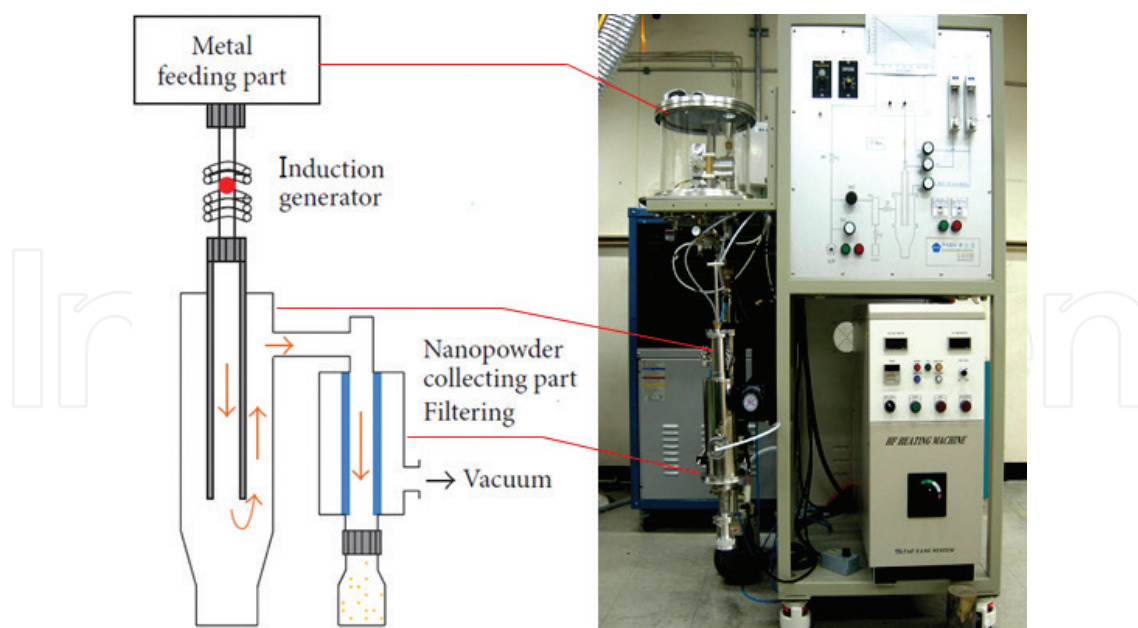


Figure 2. The concept of system for LGC.

that of Ni (1450°C). However, the high magnetic permeability of Ni affects the magnetic force and levitation of the melted droplets. Accordingly, the input power for Ni needs to be increased up to 6 kW, the maximum power for the inductor. Preparing pure Ti nanopowders using the LGC is impossible. To do so, the temperature of the inductor must be increased up to 2000°C; however, the starting materials have to be very thin and strongly passivated by a layer of titanium oxide. The seed materials need to be fully melted before levitation, because only liquid seeds can be suspended in the inductor, due to their lower density. However, it takes too long time to melt the Ti seed to produce liquid droplet for levitation.

We also supplied the starting materials for the melted liquid droplet during synthesis. We utilized a metal wire feed system, which is very convenient for fabricating nanopowder continuously. The amount of material fed over time can be controlled. The average size of the nanopowder is increased with increasing feed speed because of the increased amount of material introduced to the liquid droplet. The optimal feeding speed is between 10 and 30 mm/s during fabrication. If the feeding speed is very slow, below 10 mm/s, the size of the liquid droplets decreased, and they disappear. In contrast, if the feeding speed is increased to over 30 mm/s, the prepared powders have a wire shape because the particles are connected with each other. By adding oxygen to the inert gas, metal oxide particles or metal particles oxidized on the surface may be obtained. **Figure 3** shows metal and metal oxide particles prepared by LGC. The gas condensation (GC) method was used to obtain nanocrystalline powders of pure metal and nano-oxides with different compositions. Oxide nanopowders, such as Fe_3O_4 , $\gamma\text{-Fe}_2\text{O}_3$, and Cu_2O , were produced by the LGC of metal wires at elevated pressure in an $(\text{Ar} + \text{O}_2)$ atmosphere [8, 16].

High-purity Ni@C and Fe@C nanopowders were synthesized using the LGC method. The LGC apparatus consisted of a high-frequency induction generator, operating at 6 kW for Ni and 5 kW for Fe, a reaction chamber for the levitated liquid seed, and a unit to control the

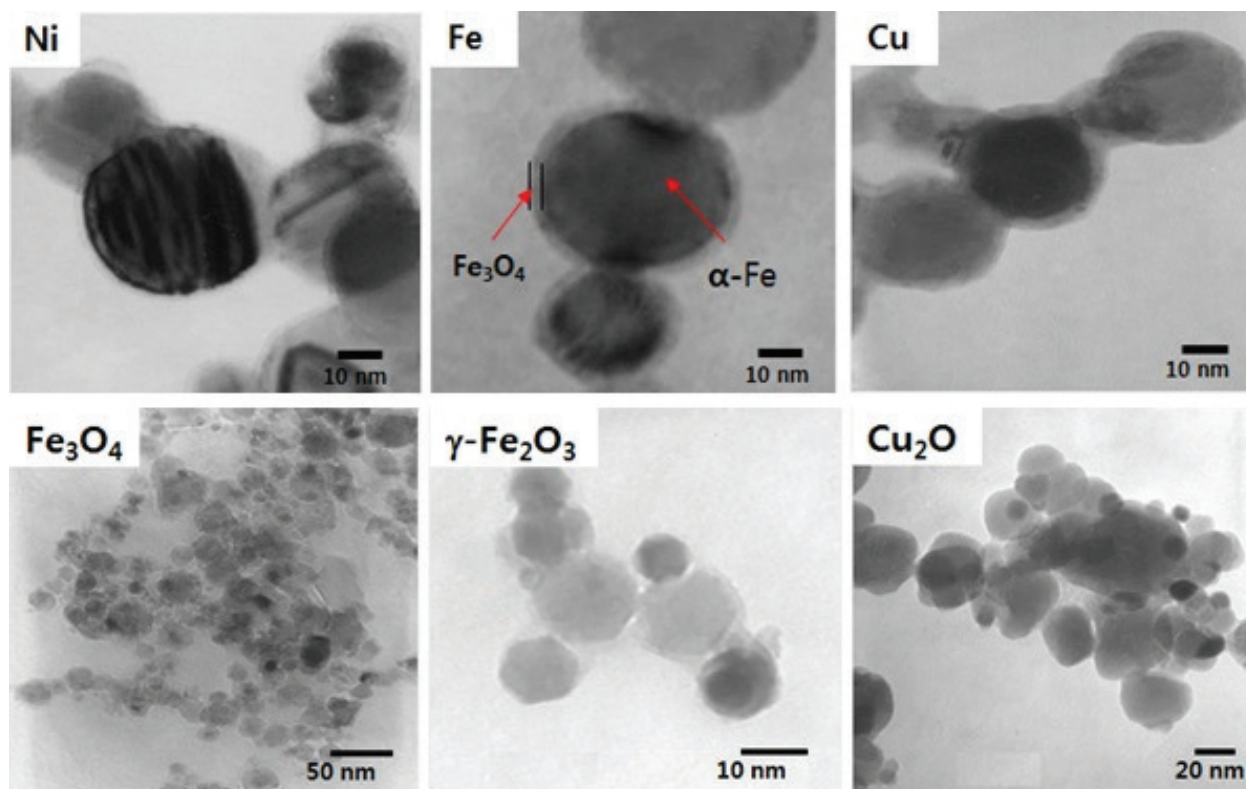


Figure 3. TEM images for metals and ceramic nanopowders.

methane (CH_4) concentration. The starting materials were Ni and Fe wires with a diameter of 4 mm. The Ni and Fe wires were fed into a melted droplet using the wire feeding system at a feeding rate of 2 mm/min. An ingot of 85 mg, which was used as the seed material for the levitation and the evaporation reactions, was melted by using electric induction. The pressure of the mixed Ar and CH_4 gas in the chamber was 100 Torr. CH_4 was 10% of the mixture gas. The inductor was heated up to a temperature of 2000°C , and the metallic atoms were evaporated from the overheated surface of the liquid droplet and condensed by cold inert gas and then collected into the filter. At the same time, the molecular CH introduced into the chamber was converted to atomic C and H with high activity under high temperature. The highly active C atoms react with the Ni and Fe atoms, and the H atoms are converted to H_2 molecules. The newly created H_2 gas is vented out of the reaction chamber by continuous vacuum operation. The results indicated that all of the as-made materials were composed of nanocapsules with uniform particle size at and below 10 nm. The nanocapsules consisted of outer multi-shells of carbon [26–28].

2.2. Starting materials with a melting temperature below 900°C : Zn, Sn, Bi, and ZnO

For most metals, the optimal design of the material heating method allows a metal drop to be heated and kept in a noncontact condition in the evaporation zone by high-frequency magnetic field. However, this method does not ensure the optimal heating of light-volatile metals such as Zn, Sn, and Bi. Therefore, another material evaporation method using a refractory crucible was applied, for heating and evaporation. This method is generally suitable for

evaporating materials with high vapor pressures at moderate temperature. **Figure 4** shows a simple diagram of the device for obtaining light-volatile metal nanopowders. The apparatus consists of a high-frequency induction generator operating at 2.5 kW, a levitation and evaporation chamber, and an oxygen concentration control unit [11]. The wire feeding velocity (V_{Zn}) and mixed Ar and O_2 gas pressure in the chamber were 50 mm/min and 100 Torr, respectively. The mechanism of ZnO formation using the LGC method was analyzed. First, a liquid droplet, which is levitated against gravity by the magnetic force due to the coupled induction coils, is heated up to the temperature of 1560°C at 2.5 kW. Then Zn clusters are evaporated from the overheated surface of the liquid droplet and condensed by cold inert gas and collected into the filter. At the same time, molecular O_2 introduced into the chamber is converted to atomic O with high activity under high temperature. The highly active O atoms can diffuse into the Zn clusters and react with the Zn atoms. A large amount of the Zn phase was observed at and below an oxygen flow rate of $V_{O_2} = 0.05$ l/min, whereas mixtures of ZnO and small amounts of the Zn phase were observed under O_2 flow rates in the range from $V_{O_2} = 0.11$ l/min to $V_{O_2} = 0.21$ l/min. However, at and above 0.21 l/min of O_2 flow rate, levitation was impossible. Some metals, such as Bi and Sn, have insufficient tensile strength to prepare wire. In these cases, the micron-sized powders were used as the parent materials. The powder starting materials were supplied by a powder feeding (PF) system. A detailed explanation of the PF is provided in Section 2.3.

Bi powders were prepared using metal bismuth powder as the starting material [28]. The powder was supplied by the feeding system into a graphite crucible at a rate of 20 mg/min. The crucible was heated by induction currents up to $T = 700$ – 900°C . Bi particles entering the crucible were evaporated within 1–2 sec and carried by argon flow from the hot zone. The argon flow rate was varied in the range of 80–170 l/h, at pressures in the range of 70–300 torr. The dependence of the mean sizes of the bismuth particles on gas pressure at a flow rate of 80 l/h was 25, 70, and 120 nm for 70, 150, and 300 torr, respectively. Thus, the optimal conditions for obtaining Bi powder were realized at an argon pressure of 70 torr and a rate of 80 l/h. A simple diagram of the process for forming nanoparticles from light-volatile seed in a crucible to produce volatile nanoparticles is represented in **Figure 5**.

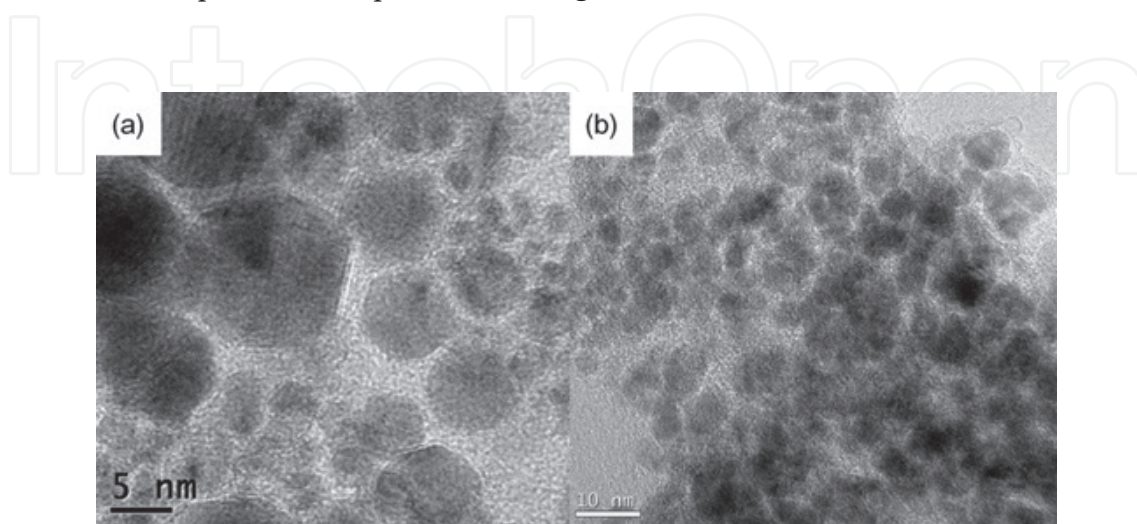


Figure 4. High-resolution TEM images of carbon encapsulated (a) Ni and (b) Fe.

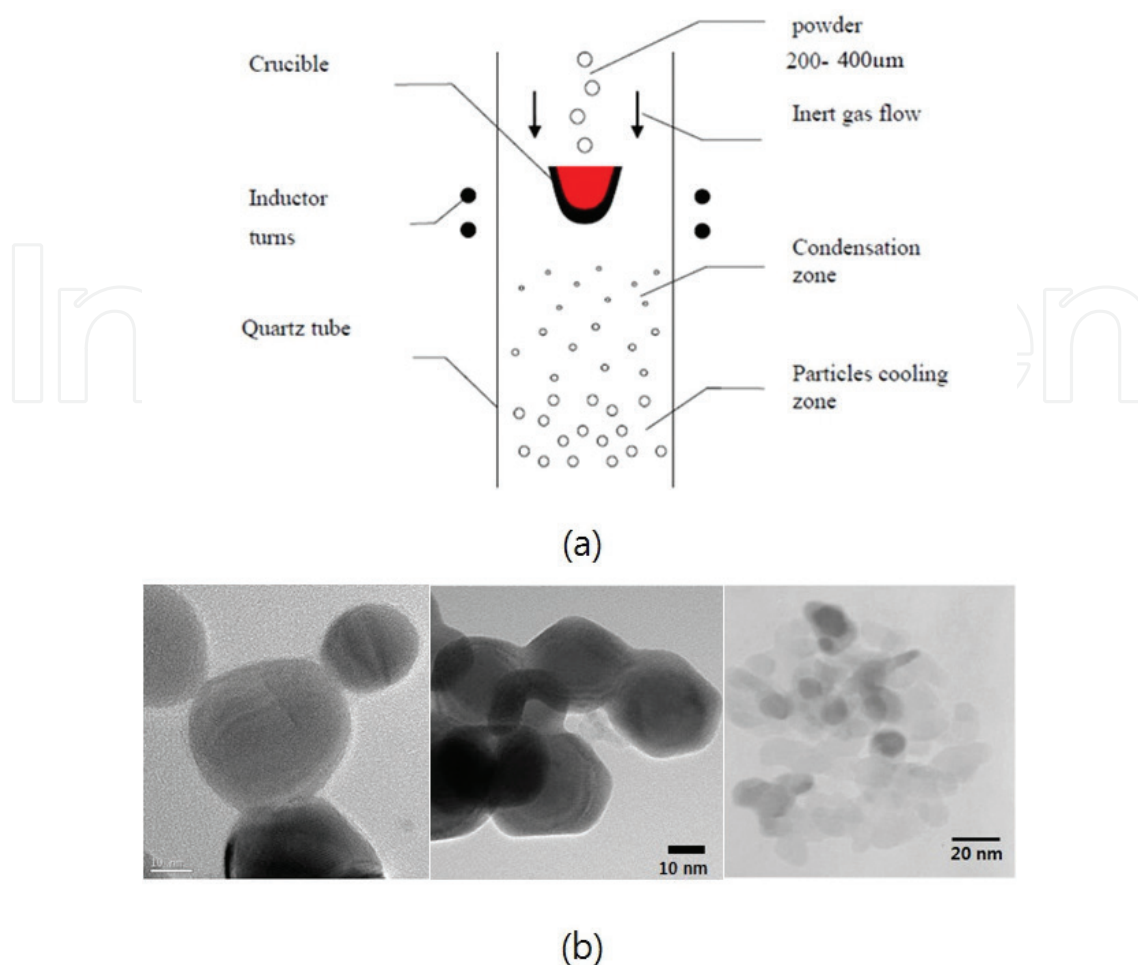


Figure 5. (a) Elementary diagram of the process for forming nanoparticles from light-volatile seed in a crucible and (b) TEM images for the Sn, Bi, and ZnO nanoparticles prepared by LGC using light-volatile seed.

2.3. Powder starting materials: NiFe₂O₄ and Ti-Ni

The wire feeding (WF) system was used for synthesizing metal, ceramic, and carbon-encapsulated materials. This system easily supplies seed parent materials continuously. However, it was impossible to synthesize several complicated metal-doped materials such as ferrites, perovskite, garnet, metal-doped ZnO, Ti-Ni, and Al-Ni-Co using the wire feeder in the LGC system, because the parent materials could not be prepared as wire. A newly modified micron powder feeding (MPF) system overcomes this problem of the LGC system [15, 20]. The MPF system can be used for synthesizing brittle metals, alloys, and complex doped materials. Commercial elemental powders of Ti (99.9 at.%, ~500 μm), Ni (99.9 at.%, ~500 μm), and Fe (99.9 at.%, ~500 μm) were used as the starting powders for the synthesis of Ti-Ni alloy and Ni-ferrite nanopowder, using the LGC. The Ti and Ni powders were mixed by pestle and mortar to achieve the desired equi-atomic composition and were then incorporated into the micron powder feeding system, which consisted of a rotating part to supply the Ti and Ni micron powders to the melted droplet and a vibrating part for mixing the powder. The Ti and Ni micron powders were fed into the powder feeding system at a feeding rate of 38 mg/min. An 83 mg Ti-Ni alloy ingot, which was used as the seed material for the levitation and

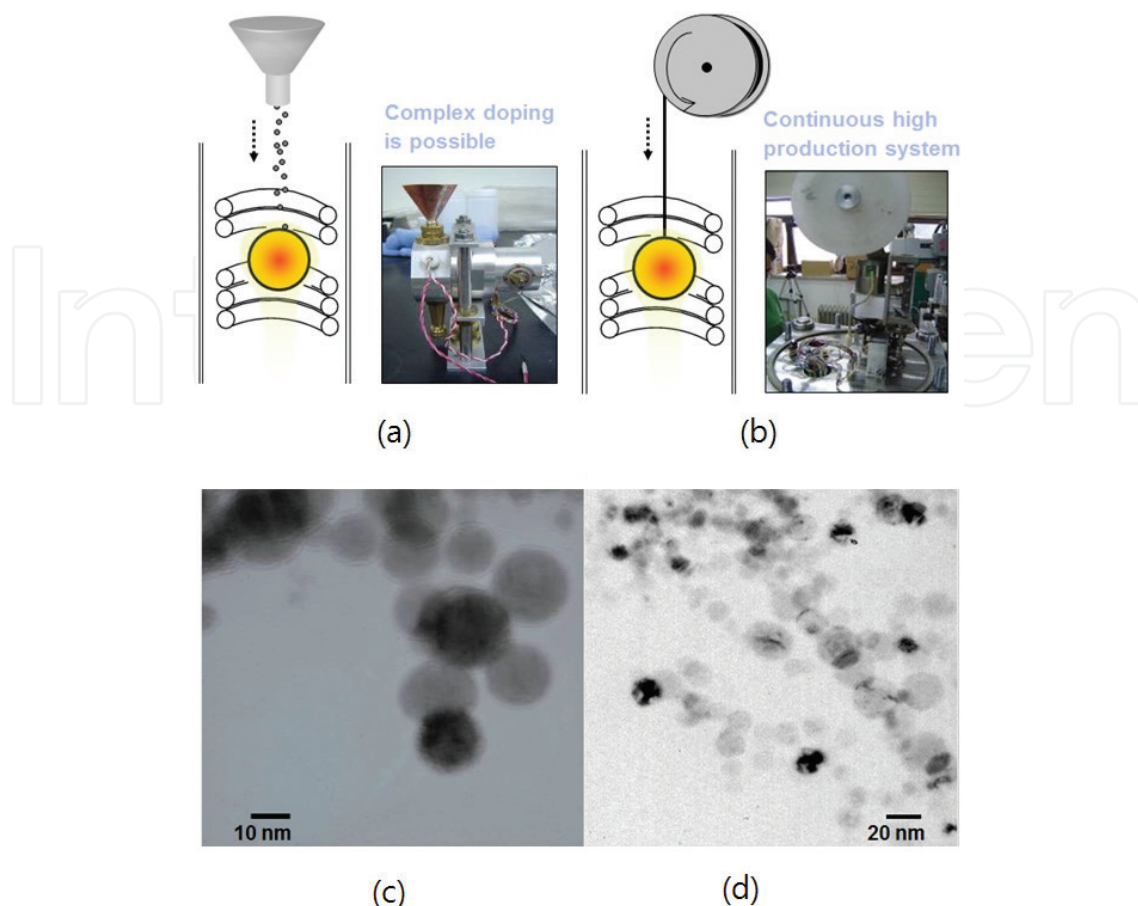


Figure 6. (a) Micron powder feeding (MPF) system and (b) wire feeding (WF) system in the LGC instrument. TEM images for (c) Ti-Ni alloys and (d) NiFe₂O₄.

evaporation reactions, was melted by an electric induction heating with an applied power of 6 kW at an argon gas pressure of 100 torr. The evaporated powders were filtered and finally passivated by partial oxidation. The starting materials were the mixed micron powders of Ni and Fe, which has a size ranging from 100 to 500 μm . The amount of micron powder fed into the liquid seed droplet was controlled at 80 mg/min. The mixed Ar and O₂ gas pressure in the chamber was 100 torr [15, 20] (Figure 6).

3. Magnetic metal and carbon-encapsulated metal nanoparticles

3.1. Magnetic properties of Ni, Fe, Ni@C, and Fe@C

Magnetic nanoparticles have attracted much attention because of their use in nano-fluids for biomedical application, thermally conductive fluids, various catalysts, etc. However, metallic nano-fluids end to be inherently vulnerable to oxidation, dissolution, and agglomeration during synthesis. In particular, agglomeration of the particles in a solvent is a serious problem when preparing nano-fluids. To overcome these problems, encapsulating the particles in a protective shell has been recommended to improve the chemical stability of the metal

nanoparticles and their dispersion stability in the solvent. It is also worth noting that after encapsulation with a carbon coating layer, these materials are not prone to agglomeration because the coating reduces their magnetic interaction. In addition, the surface diffusion processes can preserve the chemical and structural properties of the nanopowder for a long time in many chemically aggressive conditions. A graphitic carbon shell in particular is regarded as an ideal coating since it is light and shows high stability in both chemical and physical environments [29–31].

The contents of the Ni and Ni@C nanoparticles synthesized by LGC using the micron powder feeding system were confirmed by XRD pattern. The XRD results for Ni and Ni@C showed the lattice parameters and the positions of the main peaks of the Ni powders. A small amount of NiO phase and amorphous graphitic layers was found in the XRD patterns and in the TEM images as mentioned in Section 1 [18]. The diffraction peaks at 44.4° , 51.8° , and 76.3° are due to the (1 1 1), (2 0 0), and (2 2 0) planes of fcc-Ni, respectively. The Ni powders synthesized by the LGC method showed low saturation magnetization. These results were attributed to the spin-canting effect and oxide phase on the surface [32]. The magnetic properties would be weak due to the antiferromagnetic NiO phase on the powder surface. The saturation magnetization was $M_s = 42 \text{ emu/g}$, as shown in **Figure 7(a)**. The slightly shifted hysteresis loop for the Ni sample can be explained by exchange bias between the ferromagnetic core of Ni and the antiferromagnetic surface of the NiO. The initial magnetization curve is not explained by the size effect. In previous studies, the virgin magnetization curve slightly spills over the limited hysteresis loop at 655 Oe. We assume that this effect is enhanced when the size of the particles is reduced, as suggested in a previous study. With decreasing particle size, the defects and the different magnetic structure on the surface of the particles are increased. The nature of this irreversibility in high magnetic fields follows a physical model and can be explained by a spin-glass or spin-canting behavior. The hysteresis loop of the as-made M@C materials in magnetic fields up to 2 T reveals their intrinsic magnetic behavior, indicated by the magnetization (M), the remanent magnetization (M_r), and the coercive force (H_c) of the M@C samples. The saturation magnetization demonstrates that

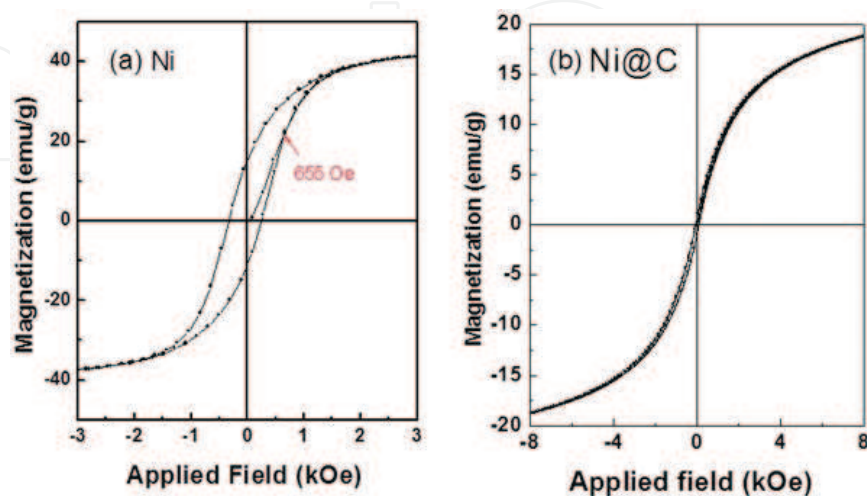


Figure 7. M-H loops for (a) Ni and (b) carbon-encapsulated Ni measured at 20°C .

the carbon-coated Ni nanocrystallites exhibited a superparamagnetic behavior at room temperature, which is related to the demagnetization effect arising from the additional energy of the magnetic fields outside the graphitic carbon encapsulation as shown in **Figure 7(b)**. The coercive force (H_c) and magnetization (M) were 76.6 Oe and 19.6 emu/g, respectively. The ratio of remanence to the saturation magnetization (M_r/M) was 0.04. The low magnetization compared with the Ni nanoparticles without the carbon shell is due to the coexistence of nonmagnetic carbon and the large percentage of surface spin due to the disordered magnetization orientation of the nanoparticles. The magnetic properties are influenced by both the particle size and the surface properties of the particle [33, 34].

A typical hysteresis loop of the Fe nanopowder at room temperature shows a saturation magnetization of $M_s = 157$ emu/g and coercivity of $H_c = 836$ Oe as shown in **Figure 8(a)**. An estimated single domain size of 14 nm for spherical iron particles with no shape anisotropy is reported. The size of the iron nanopowder is large enough to show very large value of coercivity. The hysteresis loops of the as-made Fe@Cs in magnetic fields up to 1 T reveal their intrinsic magnetic behavior, as shown in **Figure 8(b)**.

The hysteresis loops indicate that the carbon-coated Fe nanocrystallites exhibit superparamagnetic behavior at 50 and 300 K. The magnetization was not saturated in the applied fields up to 1 T, as shown in **Figure 6(b)**. In the nanoparticles, one can observe superparamagnetic behavior, which is related to the demagnetization effect arising from the additional energy of the magnetic fields outside the graphitic carbon encapsulation. The coercive force (H_c) and the magnetization (M) at 50 K were 130 Oe and 69.6 (emu/g), respectively. In a previous study, the Mössbauer spectrum for Fe@C nanopowder was measured at room temperature. The relative fraction of the α -Fe, Fe₃C, and γ -FeC phases was determined to be about 27.6, 26.3, and 46.1%, respectively. The low magnetization compared with metal nanoparticles without a carbon shell was due to the coexistence of nonmagnetic carbon and the large percentage of surface spins due to the disordered magnetization orientation of the nanoparticles. The magnetic performance of the Ni@C and Fe@C samples was demonstrated in a liquid

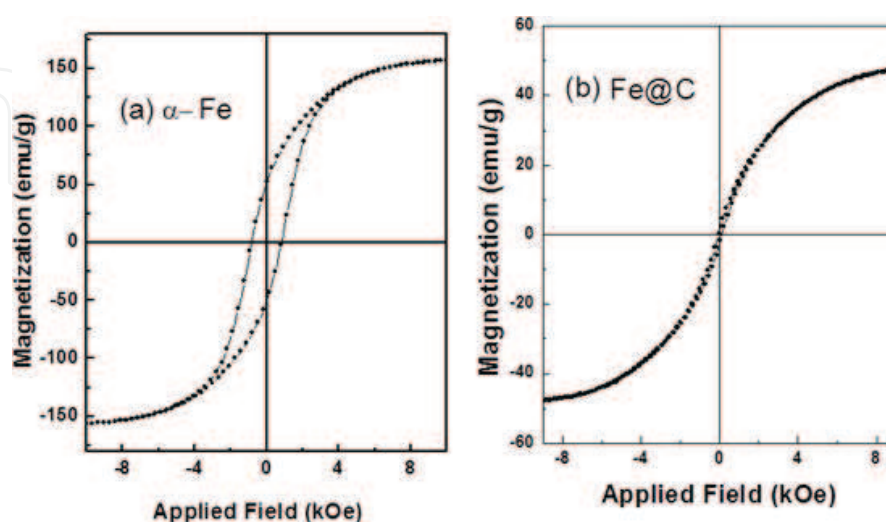


Figure 8. M-H loops for (a) α -Fe and (b) carbon-encapsulated Fe measured at 20°C.

phase (in ethanol and polyethylene glycol) by placing a magnet bar near the glass bottle. The carbon-encapsulated magnetic metals moved under the magnetic force. This suggests that Ni@C and Fe@C materials would be ideal adsorbents and catalyst supports because they are magnetically separable [35].

3.2. Dispersion stabilities of Ni, Fe, Ni@C, and Fe@C

To evaluate the dispersion stability and agglomeration phenomena of the carbon-encapsulated Ni and Fe nanoparticles in solvents of ethanol and ethylene glycol (EG), their time-dependent sedimentation behavior was investigated using transmission profile measurements obtained with a Turbiscan Lab [36–38]. The transmission profiles were taken every 1 h for 60 h when the suspending medium was ethanol. It was found that the transmission intensity decreased at the sample top owing to clarification and increased at the sample bottom due to sedimentation. A very stable Ni@C dispersion was observed without showing any clarification or sedimentation in EG. In contrast, a progressive fall signal was observed as a function of time in the middle region of Ni nanoparticles which had an average particle size of 20 nm. This can be explained by flocculation-induced particle growth. **Figure 9(a)** shows the Turbiscan screen data taken every 1 h for 3 days. The time-dependent transmission rates on the top, middle, and bottom show the same tendencies. The clarification in the top region and the progressive fall in the middle region of the ΔT signal were not observed in all suspensions. These imply that flocculation due to a coalescing reaction between the nanoparticles was insignificant. A very stable Fe@C dispersion, without any clarification on the top layer or sedimentation on the bottom layer, was observed in ethanol and EG. The viscosity of the solvent affected the dispersion stability kinetics. The dispersion stability of the solvents increased in the following order: water, ethanol, and ethylene glycol (or poly ethylene glycol). **Figure 9(b)** shows the effect of the solvent on the dispersion stability, as measured by using Turbiscan Lab, as well as the calculated mean value of the kinetics for each transmission (ΔT) profile as a function of time. The suspensions prepared in water displayed a rapid change in the mean ΔT values. As a result, sedimentation of the Fe@C nanoparticles in suspensions of water commenced as soon as the suspension was prepared. For the suspensions prepared in ethanol and EG, the variation in the mean ΔT was much less. However, this value increased continuously. Visual inspection confirmed that the suspension was stable, but sedimentation slowly occurred. However, coalescence between the Fe@C nanoparticles rarely occurred in the suspension because the carbon shell layer prevented agglomeration of the particles. The variation in the mean ΔT for the suspension prepared in EG was the smallest. The mean value of ΔBS increased when the particles were smaller than the wavelength of the incident light (880 nm). The tendency of ΔBS was similar to those of ΔT . From these results, for three kinds of solvent, we determined EG to be the most suitable solvent [38, 39].

3.3. Catalyst for the multicomponent Biginelli reaction

In this study, we introduce the catalytic effects of the Ni and Ni@C nanopowders observed during the synthesis of S-enantiomer from 3,4-dihydropyrimidine (DHPM). The synthesis

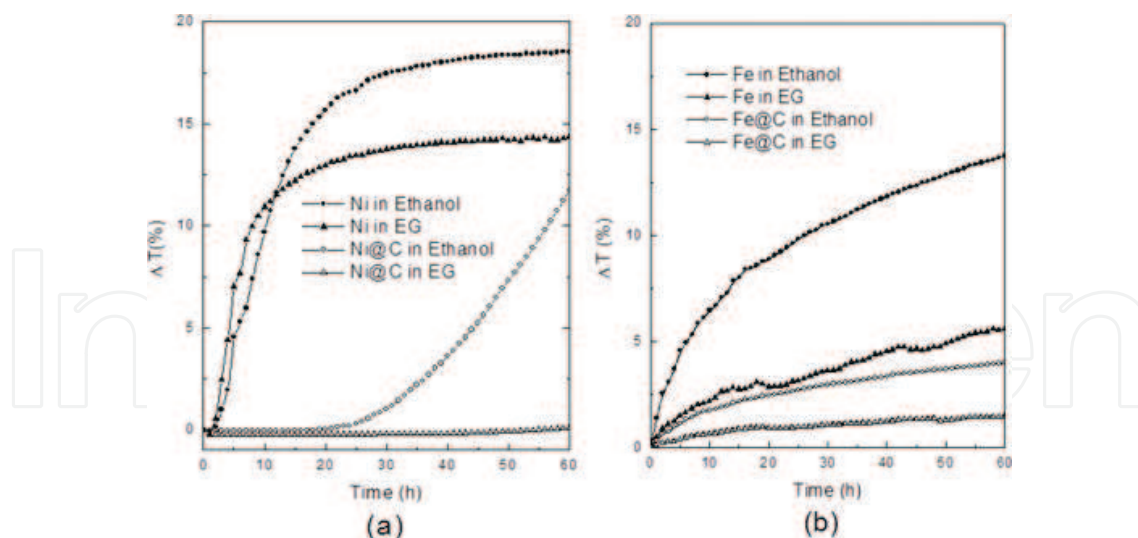
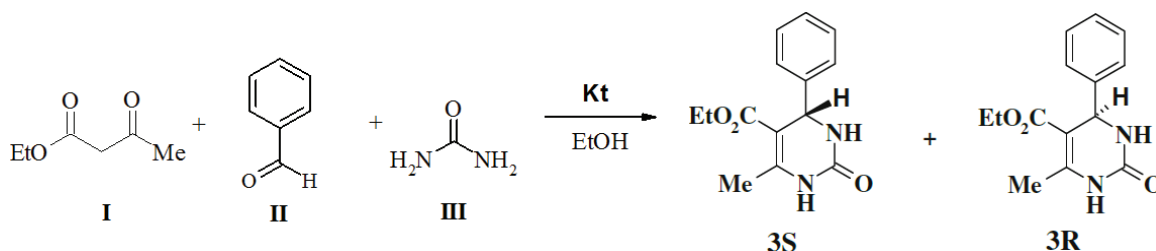


Figure 9. Variations in the mean ΔT for the (a) Ni and Ni@C suspensions and (b) Fe and Fe@C suspensions prepared in various solvents (ethanol and ethylene glycol).

of 4-Aryl-substituted DHPM compounds by the Biginelli reaction has attracted great attention in synthetic organic chemistry due to their pharmacological and therapeutic properties such as antibacterial and antihypertensive activity as well as their behavior as calcium channel blockers. Given the versatile biological activity of DHPM, development of an alternative synthetic methodology is of paramount importance [40–42]. This has led to the development of several new synthesis strategies involving combinations of Lewis acids and transition metal salts such as mainly homogeneous catalysts, which give high yields. However, in spite of their potential utility, many of these methods involve expensive reagents, long reaction times, high temperatures, and stoichiometric amounts of catalysts and result in unsatisfactory yields. Therefore, discovering a new, inexpensive catalyst for the Biginelli-type reaction under neutral and mild conditions is of prime importance. The starting materials used in this study were ethyl acetoacetate (I) (0.25 mmol), benzaldehyde (II) (0.25 mmol), and urea (III) (0.3 mmol). First, the benzaldehyde (II) (0.25 mmol), urea (III) (0.3 mmol), 0.1 g of catalyst (Ni or Ni@C), and chiral modifier of L-proline (0.025 mmol) were mixed and react in ethanol (50 ml) at 70°C for 2 hours. In the second step, ethyl acetoacetate (I) (0.25 mmol) was added and reacted under microwave for 3h. The ratio of the *s*-enantiomer in the as-prepared sample was characterized by high-performance liquid chromatography (HPLC) with a chiral column (Chiralcel OD-H) [13].



Catalysts	Yield (%) Racemic	HPLC		Δ (ee. %)
		S-enantiomer	R-enantiomer	
Ni	47	53.2	45.8	7.4
Ni@C	70	59.8	40.2	19.6

Table 1. Synthesis of 3,4-dihydropyrimidine based on the Biginelli reaction using nanosized catalysts of Ni and Ni@C.

Vigorous agitation appeared to be an extremely important factor influencing stereo selectivity. The results of stereo selectivity are represented in **Table 1**. The simultaneous use of a heterogeneous catalyst along with the chiral modifier allowed the ratio between stereoisomer in the Biginelli reaction to be changed in some experiments in favor of the S-enantiomer, with an excess of about 19.6%. The best results were obtained when using carbon-encapsulated Ni nanoparticles as the catalyst, L-proline as the chiral modifier, and methanol as the solvent. The catalytic reaction with Ni@C showed higher stereo selectivity than with Ni. The carbon shell influences the catalytic effect during synthesis [43].

4. Nonmagnetic metal and metal oxides: Cu oxide, Bi, and NiO

4.1. Catalytic activities of Cu oxide and ZnO

Cu oxides are widely applied in various organic syntheses such as reduction and oxidation processes, various condensation processes, for the syntheses of complex compounds, etc. The surface of the nanocrystalline Cu oxide includes a defect structure, resulting in non-stoichiometry. Such materials in themselves have the advantages of both homogeneous and heterogeneous catalysts. The aim of our investigation was the development of an effective catalytic and reaction systems based on nanocrystalline Cu oxides, with high reactivity at ambient temperature. To test the catalytic reaction, both the reaction of the liquid-phase oxidation of 2,3,5-trimethyl-1,4-hydroquinone (TMHQ) and the catalase activity were chosen. The oxidation of TMHQ is an intermediate stage of the hydroxylation of 2,3,6-trimethyl phenol in the synthesis of tocopherol. The process of TMHQ oxidation was carried out in a thermostatically controlled chamber, under agitation in a mixed water and methanol solution (1:1 in volume) at $50 \pm 0.2^\circ\text{C}$. The rate of air supply was 6.2 l/h. The reaction was carried out using the parent material (0.66 mmol) and the nanopowders (1 mmol). To compare the catalytic properties of the Cu oxides, powders with various sizes were synthesized. The size control of the powder was carried out by altering the feeding velocity of the Cu wire from 20 to 80 mm/min. Phase control of the Cu, Cu₂O, and CuO was carried out by controlling the pressure of the inert gas. In **Table 2**, the crystallite conditions of the copper oxides are displayed. The dehydrogenation (oxidation) of the TMHQ in solution was to practically form 2,3,5-trimethyl-1,4-quinone (TMQ) (selectivity on TMQ > 99.5%). The kinetic curves of TMHQ oxidation in the presence of the nanocrystalline Cu oxide particles (Samples 1, 2, and 3) are given in **Figure 10**. Samples containing mainly pure Cu (Cu 78%, Cu₂O 22%, sample a)

	Average particle size (nm)	Conditions for synthesis: feeding speed, draft velocity (l/min), and pressure in chamber	Phase composition, wt. %			Oxidized yield of TMHQ	H ₂ O ₂ conversion
			Cu	Cu ₂ O	CuO		
a	20	Slow feeding (20~30 mm/s) 0.0 ≤ V _{O₂} ≤ 0.05, 80 torr	78	22	—	No reaction	10.2
1	90	Fast feeding (60 mm/min) V _{O₂} = 0.2, 120 torr	4	96	—	Initial	60.1
2	35	Slow feeding(20~30 mm/min) V _{O₂} = 0.2, 100 torr	—	100	—	Active	99.8
3	35	Slow feeding (20~30 mm/min) 0.1 ≤ V _{O₂} ≤ 0.15, 100 torr	10	85	5	Active	82.3

Table 2. The concentration of Cu oxide nanopowders, the reaction yields for dehydrogenation of TMHQ, and hydrogen peroxide (catalase activity).

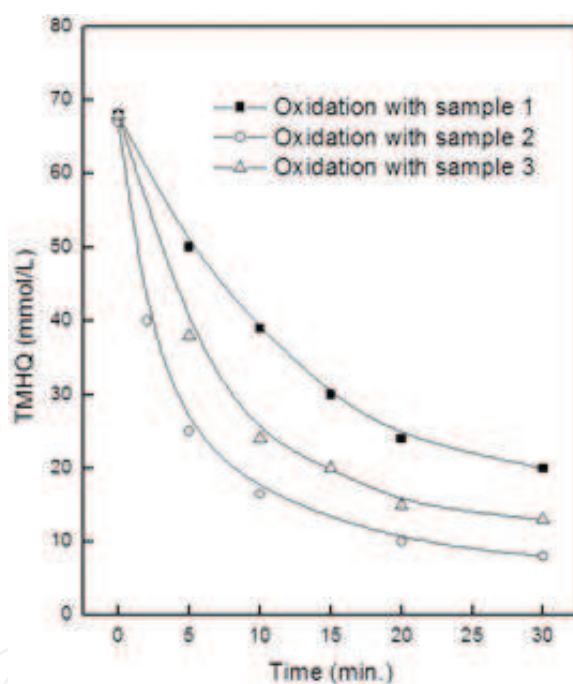


Figure 10. Kinetic curves for the dehydrogenation of TMHQ using Cu oxide catalysts with average particle size of 35 and 90 nm.

in the structure showed rare catalytic reaction. Catalytic activity depended on both the average particle size and the oxide phase such as the concentration of Cu₂O in the nanopowders. Sample 1 with mainly Cu₂O phase and an average size of 90 nm performed as catalyst with theoretical yield. Samples 2 and 3 with an average size of 35 nm showed significantly active effect. These samples contained a small quantity of CuO, not exceeding 0.15 mol fraction. The results of the oxidation of TMHQ are represented in **Table 2**. The catalytic yield of Sample 1 compared with Samples 2 and 3 was relatively very low. The Samples 2 and 3 with the same range of particle sizes included different ratios of Cu and Cu oxide phase. The yield of

TMHQ oxidation depended on the particle size and amount of the Cu_2O phase. Obviously, oxidation of the parent material substantially occurred under the action of the fixed oxygen, which was activated in the matrix of nanopowders [44–46].

The catalase activity is an informative parameter about the catalytic properties of the materials in the redox process. It was simulated by measuring the ability of the catalase in the decomposition of hydrogen peroxide to isolate molecular oxygen. Decomposition of the hydrogen peroxide was carried out in a thermostatically isolated chemical reactor (10 ml). A mixture of water and methanol (1:1 in volume) was agitated with a stirring rod at $50 \pm 0.2^\circ\text{C}$. The reaction was carried out with hydrogen peroxide (1.7 mmol) and nanopowder (2 mg). The catalytic activity of the Co, Mn, Fe, and Cu hydroxides was also estimated by catalase activity. The aim of this work was to solve a scientific problem related to the chemical intoxication mechanisms of water phenol solutions and its derivatives during their cleaning. The data in **Table 2** show the results of the catalase activities for the same nano-Cu oxide samples. The reaction of Sample 2 with a size of 35 nm, containing mainly Cu_2O , showed much higher activity than Sample 1 with a size of 90 nm and the same oxide phase. The size of the particles was the most significant factor. The particle size affects the surface state. The specific surface areas of Samples 1, 2, and 3 were 17, 35, and $38 \text{ m}^2/\text{g}$, respectively. The specific surface area is related to the particular manufacturing method. The LGC method produces nano-scaled powders with high specific surface area [47].

The photocatalytic activity of the ZnO was evaluated based on the photodegradation of phenol aqueous solutions under different irradiation conditions. For experiments under UV-visible light, 100 mL of 50 ppm phenol in aqueous solution with 0.5 g catalytic powders was loaded in a glass container and stirred with a magnetic stirrer under irradiation from a Hg-Xe lamp. Total organic carbon (TOC) values as a function of time were measured after filtration under reduced pressure. **Figure 11** shows the photo mineralization of phenol with UV-visible light (solar simulator) in the presence of ZnO. Obviously, when ZnO is added to the phenol, the total organic carbon (TOC) value was reduced to 60% [48–51].

4.2. Electrochemical analyses using Bi nanopowder

The anodic stripping voltammetry (ASV) method is a powerful electrochemical technique for trace metal analysis. The traditional electrodes for ASV measurements are mercury-drop electrode and a mercury-film electrode, due to high sensitivity of the mercury [52–56]. However, mercury is very toxic. The toxicity of the mercury has led its usage to be completely banned in some countries. In this study, we focused on searching for alternative environment-friendly electrode materials. The Bi-film electrode has been considered replacing the mercury-film electrode due to its nontoxicity. The properties of Bi materials show not only excellent resolution of neighboring peaks but also insensitivity to the dissolved oxygen in the solution. However, there are still some problems to use the electrode such as a low detection limit comparing to mercury electrode and complication of preparing electrode including processes of additional washing or polishing of the carbon surface and dissolving Bi ions into the solution for the pre-deposition of the Bi on the film electrode. In order to overcome the above weaknesses of the Bi-film electrode, a Bi nanopowder-labeled electrode with

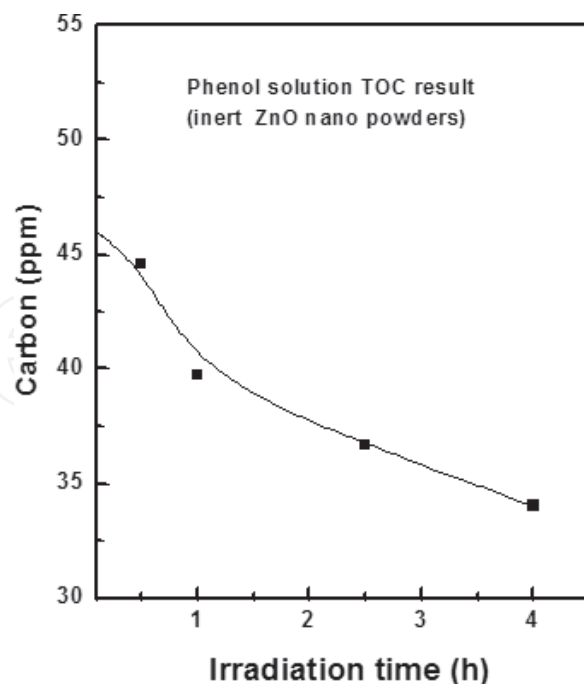


Figure 11. Photo mineralization of phenol with sunlight (TOC: total organic carbon content at times) in the presence of ZnO (Hg-Xe lamp with a wavelength of 200 ~ 2500 nm and 1 kW of power).

a larger electrochemical active surface area was fabricated [57–59]. In this study, the nano-Bi-fixed electrode sensor and a nanosized Bi-binding technology were developed to improve the electrochemical characteristics of Bi for detecting heavy metals. For this purpose, the Bi nanopowder was synthesized using the LGC method and was then coated on a conductive carbon layer using a Nafion solution. **Figure 12** illustrates the attached Bi working electrode and the analysis system setup for measuring Zn, Cd, Pb, and Ta [14, 24, 58–62].

The working electrode was prepared using conductive carbon ink (DongYoung Chemical Co., LTD, in South Korea) painted flexible polyester film by a semiautomatic screen printing instrument. Then the prepared carbon ink with a thickness of 80 μm on painted thick film was

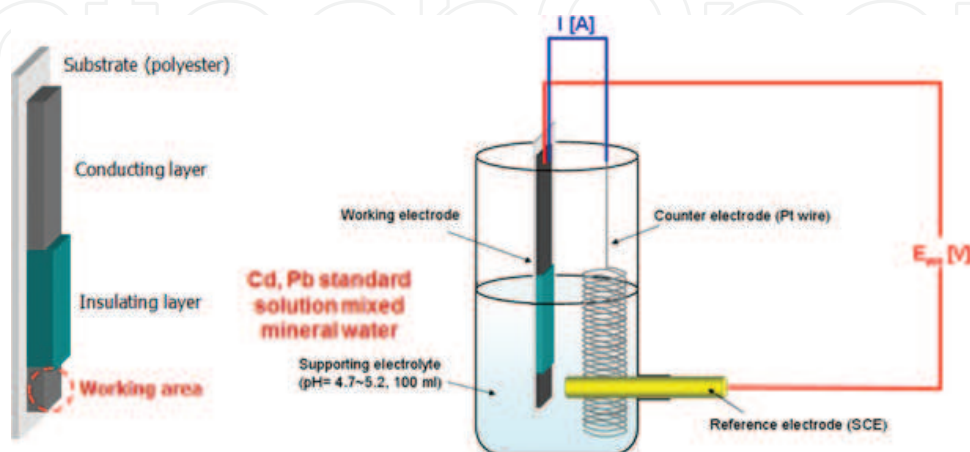


Figure 12. Illustration for working electrode and total system for electrochemical analyses.

partially covered by an insulating layer. Bi nanopowders were well dispersed into 20 ml of distilled water using an ultrasonic treatment. A Nafion solution (Fluka) was added in to the Bi-dispersed suspension for strong chemical bonding between nanopowder and the carbon paste. Finally, the Bi nanopowder-dispersed suspension was dropped onto the working area and dried in the air at room temperature. As the concentration of Nafion in suspension was increased, the value of pH was decreased due to the strong acidity of the Nafion.

When the Bi nanoparticles were dispersed in distilled water without Nafion, the zeta potential showed a positive value [14]. However, as Nafion was added in the suspension, the zeta potential changed to a negative value. The amount of Nafion should be optimized to be 200 μl for dispersion stability and the phase stability of Bi nanoparticles. The sensor electrodes were prepared using the screen-printed carbon surface with the Bi nanoparticles strongly attached by Nafion. A platinum wire and a saturated calomel electrode (SCE) were used as a counter electrode and a reference electrode, respectively. The supporting electrolyte was a 0.1 M NaAc and 0.025 M HCl solution of pH 5.0. The prepared nanoparticles are confirmed by XRD as shown in **Figure 13(a)**. Also, the screen-printed Bi nanoparticles dispersed in Nafion on the electrode could be observed by TEM, as shown in **Figure 13(b)**.

Figure 14 shows results of the anodic stripping voltammograms (ASV) using the Bi nanopowder-attached electrode for measuring various concentrations of Cd and Pb ions in solution. The ASV showed well-defined peaks at -0.85 V and -0.65 V corresponding to the oxidation of Cd and Pb, respectively. **Figure 15** demonstrates the dependence of the stripping peak current density I_p on the Cd and Pb concentrations over a range of 3~30 ppb (deposition potential = -1.35 V and deposition time = 3 min). From the linearity between the metal concentration and the peak current, the values of the sensitivity of the nano-Bi-fixed electrodes were determined to be 9.01 ± 0.012 and 7.15 ± 0.007 $\mu\text{A/ppb}\cdot\text{cm}^2$ for Cd and Pb, respectively. The estimated detection limits of the nano-Bi-fixed electrode were 0.31 and 0.42 ppb for Cd and Pb, respectively, on the basis of the signal-to-noise characteristics ($S/N = 3$) under a 10 min accumulation. These values are much lower than the domestic and the international content limits of Cd and Pb ions in drinking water, which are listed in **Table 3**, indicating the excellent

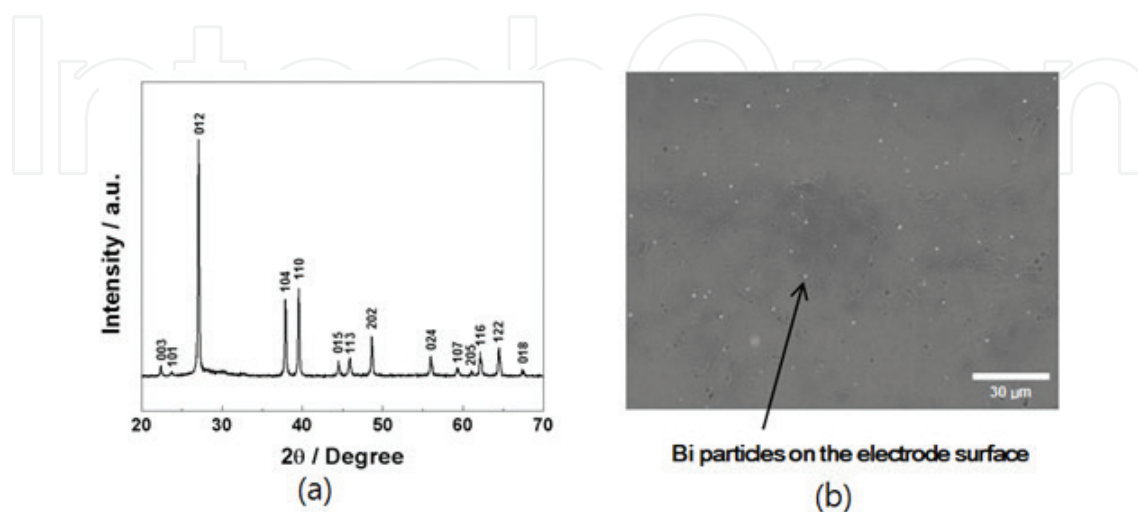


Figure 13. XRD pattern for (a) Bi nanopowders and (b) SEM image for screen-printed Bi.

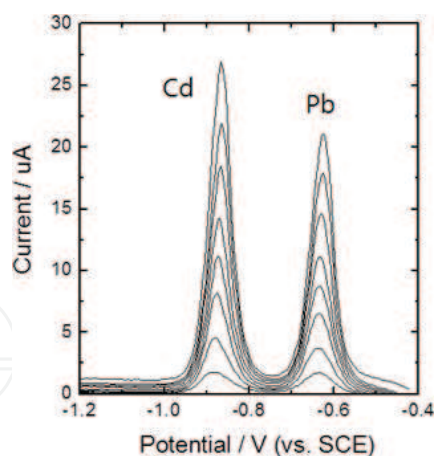


Figure 14. Square wave anodic stripping voltammograms experimentally measured on the nano-Bi-fixed electrode for various concentrations of Zn, Cd, and Pb ions.

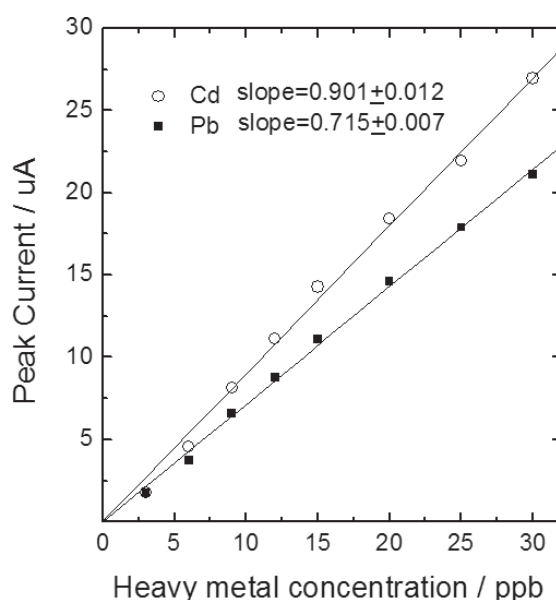


Figure 15. Dependence of the stripping peak current density I_p on the Cd and Pb concentrations over the range of 3 ~ 30 ppb (deposition potential = -1.35 V; deposition time = 3 min).

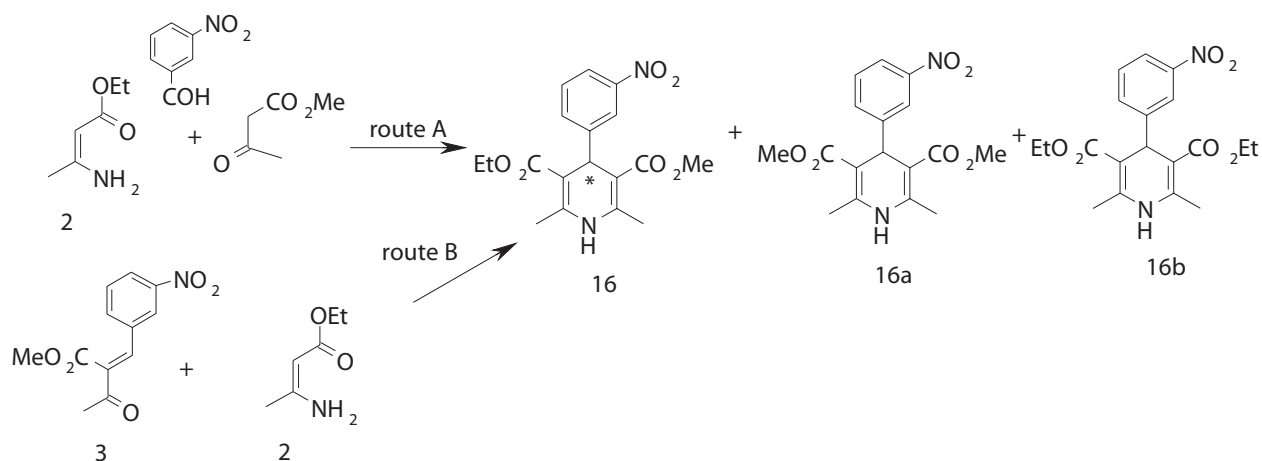
detection of the Bi nanopowder-fixed electrode. Consequently, the low toxicity of the Bi nanopowder-fixed electrode with high sensitivity about heavy metals promises the development of an attractive sensor for monitoring toxic chemical species in environmental matrices with a clean methodology [62].

4.3. Catalytic effect of NiO in the Biginelli and Hantzsch reaction

Nickel oxide powders were obtained by the gas condensation method in an argon-oxygen mixture flow. The argon flow rate was 130 l/h, oxygen concentration 8.5 vol %, pressure equal to 90 torr, and Ni feed rate 1.8 g/h. XRD analysis showed the following phase composition: NiO 90.7%, Ni 9.3%, and mean size of nickel oxide particles 13 nm. According to the electron microscopy, the particles proved to have a nearly uniaxial shape. The nickel phase detected

by the XRD method appears to result from the incomplete oxidation of some particles, and it is located in the center of the particles, while the outer layers must certainly be in an oxidized state (Figures 16 and 17).

The NiO nanoparticles were applied for the synthesis of both dihydropyridine (DHP) and dihydropyrimidine (DHPM) as mentioned in Section 3.3. The most plausible pathway for DHP prepared by the Hantzsch reaction has been shown to involve the interaction of benzaldehyde with one molecule of β -dicarbonyl compound 1 to give chalcone 3, while another molecule of β -dicarbonyl compound 1 is transformed into enamine 2. In route A, enamine 2 is condensed with an aldehyde and ethyl acetoacetate 1 in the reflux in a suitable solvent (methanol or ethanol) [63–65]. Route B involves the reaction of chalcone 3 with enamine 2, and it seems to give better yields of products and easier purification. In the presence of aqueous ammonia, compound 3 undergoes a partial decomposition into benzaldehyde and diketone 1, thus giving a rise to the formation of symmetrical analogues nitrendipine 16a, b. When the Hantzsch reaction is carried out at 22–25°C in the presence of L-proline and nanosized NiO, the ratio of enantiomers of nitrendipine is changed in favor of the S-enantiomer by 3.4%.



The Biginelli reaction for synthesizing DHPM was carried out in the presence of L-proline and nanosized NiO (obtained by the Institute of Metal Physics) to change the ratio of enantiomers of 3S in Section 2.3 is changed in favor of S-enantiomer by 15.4%. Our future plans involve studying the factors that affect enantiofacial discrimination for the Hantzsch and Biginelli reaction, such as the nature of nanosized metal oxides or chiral modifiers, reaction time, temperature, and solvent. We also plan to synthesize new nanosized metals and their oxides, as well as chiral modifiers.

Heavy metal	unit	Korea	IBWA	FDA	WHO/FAO
Cd	ppb	5	5	5	3
Pb	ppb	50	5	5	10

Table 3. Domestic and international content limits of cd and Pb ions in drinking water.



Figure 16. TEM image of NiO nanopowder.

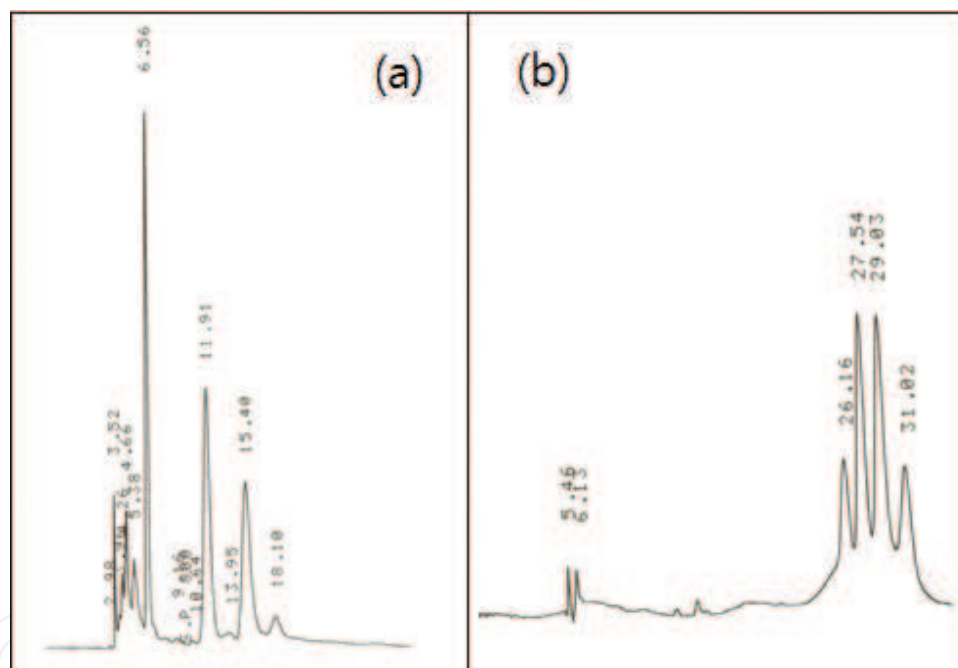


Figure 17. Chromatogram of a racemic mixture of (a) DHPM, enriched with S-enantiomer by 15.4%. The product was obtained in the presence of L-proline and NiO nanopowder mic mixture of (b) DHP, enriched with S-enantiomer by 3.4%.

5. Conclusion

Ceramics, such as NiO, ZnO, and Cu₂O, magnetic nanoparticles, including γ -Fe₂O₃, Fe₃O₄, and NiFe₂O₄, and metals, such as Cu, Ni, Zn, Sn, Ag, Au, Bi, and carbon-encapsulated metals (Ni and Fe), were synthesized by levitational gas condensation (LGC) method using wire feeding (WF) and micron powder feeding (MPF) systems. The magnetic properties have

been characterized using a vibrating sample magnetometer (VSM). The size and shape of the nanopowders were investigated by transmission electron microscopy (TEM). The surface effect influenced the magnetic behaviors of nanopowders. Bi metals were dispersed in Nafion. The Bi particles could be applied as sensor electrode instead of mercury-based electrolyte. The particle size of carbon-coated metal with diameters in the range of up to 10 nm was smaller than those of metals without a carbon shell. The dispersion stability kinetics of carbon-coated nanopowders showed good dispersion. The best results were obtained when using carbon-encapsulated Ni nanoparticles as a catalyst, L-proline as a chiral modifier, and methanol as a solvent. The catalytic reaction of Ni@C showed enhanced stereoselectivity. Also, the simultaneous use of the heterogeneous catalyst and chiral modifier may lead to an increase in the selectivity of the Biginelli reaction. Nanoparticles prepared using LGC showed significantly enhanced catalytic activities during chemical reaction due to the high level of defects on their surface structure.

Author details

Young Rang Uhm

Address all correspondence to: uyrang@kaeri.re.kr

Radioisotope Research Division, Korea Atomic Energy Research Institute (KAERI), Daejeon, Republic of Korea

References

- [1] Ruoff RS, Lorents DC, Chan B, Malhotra R, Subramoney S. Single crystal metals encapsulated in carbon nanoparticles. *Science*. 1993;**259**(5093):346-348
- [2] Scott JHJ, Majetich SA. Morphology, structure, and growth of nanoparticles produced in a carbon arc. *Physical Review B*. 1995;**52**(17):12564-12571
- [3] Lu C-H, Yeh C-H. Influence of hydrothermal conditions on the morphology and particle size of zinc oxide powder. *Ceramics International*. 2000;**26**(4):351-357
- [4] Park JB, Jeong SH, Jeong MS, Kim JY, Cho BK. Synthesis of carbon encapsulated magnetic nanoparticles by pulsed laser irradiation of solution. *Carbon*. 2008;**46**:1369-1377
- [5] Junichi N, Chie O, Osamu O, Nobuyuki N. Synthesis structures and magnetic properties of carbon encapsulated nanoparticles via thermal deposition of metal acetylide. *Carbon*. 2006;**44**(14):2943-2949
- [6] Gonsalves KE, Rangarajan SP, Wang J. In: Nalwa HS, editor. *Handbook of Nanostructured Materials and Nanotechnology*. San Diego: Academic Press Ed; 2000
- [7] Han BS, Rhee CK, Lee MK, Uhm YR. Synthesis of nano crystalline Ni and Fe by levitational gas condensation method. *IEEE Transaction Magnetics*. 2006;**42**(11):3779-3781

- [8] Uhm YR, Kim WW, Rhee CK. Phase control and Mössbauer spectra of nano γ -Fe₂O₃ particles synthesized by the levitational gas condensation (LGC) method. *Physica Status Solidi A*. 2004;**201**(8):1934-1937
- [9] Yermakov AY, Uimin MA, Mysik AA. Magnetism and structure of nanoparticles and mesoscopic systems. *Materials Science Forum*. 2002;**386-388**:455-464
- [10] Uhm YR, Lee HM, Rhee CK. Structure and magnetic properties of carbon-encapsulated Ni nanoparticles. *IEEE Transactions on Magnetics*. 2009;**45**(6):2453-2455
- [11] Uhm YR, Han BS, Lee MK, Hong SJ, Rhee CK. Synthesis and characterization of nanoparticles of ZnO by levitational gas condensation. *Materials Science and Engineering A*. 2007;**449-451**:813-816
- [12] Uhm YR, Lee HM, Rhee CK, Kim CS. Magnetic properties and dispersion stability of carbon encapsulated Fe nanoparticles. *Journal of the Korean Physical Society*. 2010;**57**(6):1609-1613
- [13] Uhm YR, Lee HM, Fedorova O, Ovchinnikova I, Valova M, Rusinov G, et al. Synthesis of carbon encapsulated metal (Ni and Cu) nano particles and applications for chiral catalysts. *Research on Chemical Intermediates*. 2010;**36**:867-873
- [14] Lee G-J, Lee HM, Uhm YR, Lee MK, Rhee CK. Square-wave voltammetric determination of thallium using surface modified thick-film graphite electrode with bi nanopowder. *Electrochemistry Communications*. 2008;**10**:1920-1923
- [15] Han BS, Uhm YR, Lee MK, Park JJ, Rhee CK, Kim GM. Synthesis of Ti₅₀Ni₅₀ alloy nanopowders synthesized by modified levitational gas condensation method. *Solid State Phenomena*. 2007;**119**:263-266
- [16] Uhm YR, Han BS, Lee MK, Rhee CK. The heat treatment of nanocrystalline Cu₂O to enhance the catalytic effect at the surface layer. *Solid State Phenomena*. 2006;**118**:635-638
- [17] Uhm YR, Lee MK, Rhee CK. Study on the catalytic properties of copper oxide nanoparticles synthesized by levitational gas condensation (LGC) method. *Journal of the Korean Magnetic Society*. 2007;**17**(2):99-102
- [18] Uhm YR, Rhee CK. Synthesis and magnetic properties of Ni and carbon coated Ni by Levitational gas condensation (LGC). *Journal of Nanomaterials*. 2013;**2013**:1-6
- [19] Uhm YR, Lee HM, Lee GJ, Rhee CK. Synthesis of metal and ceramic magnetic nanoparticles by Levitational gas condensation (LGC). *Journal of Magnetics*. 2009;**14**(2):75-79
- [20] Uhm YR, Han BS, Lee HM, Rhee CK. Synthesis and characterization of NiFe₂O₄ nanoparticles synthesized by levitational gas condensation (LGC). *Solidstate Phenomena*. 2008;**135**:123-126
- [21] Uhm YR, Park JH, Kim WW, Cho C-H, Rhee CK. Magnetic properties of nano-size Ni synthesized by the pulsed wire evaporation (PWE) method. *Materials Science and Engineering B*. 2004;**106**(3):224-227

- [22] Caoa H, Huangb G, Xuana S, Wu Q, Gua F, Li C. Synthesis and characterization of carbon-coated iron core/shell nanostructures. *Journal of Alloys and Compounds*. 2008;**448**:272-276
- [23] Liu BH, Ding J, Zhong ZY, Dong ZL, White T, Lin JY. Large-scale preparation of carbon-encapsulated cobalt nanoparticles by the catalytic method. *Chemical Physics Letters*. 2002;**358**(1-2):96-102
- [24] Lee G-J, Lee H-M, Rhee C-K. Bismuth nano-powder electrode for trace analysis of heavy metals using anodic stripping voltammetry. *Electrochemistry Communications*. 2007;**9**(10):2514-2518
- [25] Uhm YR, Park JH, Kim WW, Lee MK, Rhee CK. Novel synthesis of Cu₂O nano cubes derived from hydrolysis of cu nano powder and its high catalytic effects. *Materials Science and Engineering A*. 2007;**449-451**:817-820
- [26] Uhm YR, Rhee CK, Park J-J, Jun S-H. Morphologies and dispersion stabilities of carbon encapsulated metal (Ag and Cu) nanoparticles synthesized by pulsed-wire evaporation (PWE). *Research on Chemical Intermediates*. 2013;**39**:3387-3398
- [27] Jun S-H, Uhm YR, Rhee CK, Song R-H, Park S-J, Kim H-W. Preparation of carbon-encapsulated Ag nanoparticles for dispersion in La_{0.6}Sr_{0.4}Co_{0.3}Fe_{0.7}O_{3-δ}. *Journal of the Korean Physical Society*. 2011;**59**(6):3648-3651
- [28] Wang ZH, Choi CJ, Kim BK, Kim JC, Zhang ZD. Characterization and magnetic properties of carbon-coated cobalt nanocapsules synthesized by chemical vapor condensation process. *Carbon*. 2003;**41**(9):1751-1758
- [29] Savino V, Yann L, Rocio C, Oscar B, Brigitte B, Morales M. Continuous production of inorganic magnetic nanocomposite for biomedical applications by laser pyrolysis. *Journal of Magnetism and Magnetic Materials*. 2006;**5**(12):971-975
- [30] Xu B, Guo J, Wang X, Liu X, Ichinose H. Synthesis of carbon nanocapsules containing Fe, Ni, or co, by arc discharge in aqueous solution. *Carbon*. 2006;**4**(13):2631-2634
- [31] Jacob DS, Genish I, Klein L, Gedanken A. Carbon-coated core-shell structured copper and nickel nanoparticles synthesized in an ionic liquid. *Journal of Physical Chemistry B*. 2006;**110**(36):17711-17714
- [32] Kinemuchi Y, Ishizaka K, Suematsu H, Jiang W, Yatsui K. Magnetic properties of nano-size NiFe₂O₄ particles synthesized. *Thin Solid Films*. 2002;**407**(1-2):109-113
- [33] Yu C, Qiu JS. Preparation and magnetic behaviour of carbon-encapsulated cobalt and nickel nanoparticles from starch. *Chemical Engineering Research and Design*. 2008;**86**(8):904-908
- [34] Hayashi T, Hirono S, Tomita M, Umemura S. Magnetic thin films of cobalt nanocrystals encapsulated in graphite-like carbon. *Nature*. 1996;**381**(6585):772-774
- [35] Scott J, Majetich S. Morphology, structure, and growth of nanoparticles produced in a carbon arc. *Physical Review B*. 1995;**52**(17):12564-12571

- [36] Lee MK, Uhm YR, Rhee CK, Lee YB. Organic suspension behavior of rutile TiO₂ nanoparticles with high specific surface area. *Materials Transactions*. 2010;**51**(12):2157-2161
- [37] Park K-Y, Uhm YR, Son KJ, Park D-Y. Electrophoretic deposition of Ni nanoparticles from suspension on to a Ni plate. *Research on Chemical Intermediates*. 2015;**41**(9):6721-6730
- [38] Woo SH, Lee MK, Rhee CK. Sedimentation properties of TiO₂ nanoparticles in organic solvents. *Solid State Phenomena*. 2007;**119**:267-270
- [39] Shaw DJ. *Introduction to Colloid and Surface Chemistry*. 4th ed. London: Butterworth; 1992 306 p
- [40] Rodriguez H, Suarez M, Perez R, Petit A, Loupy A. Solvent-free synthesis of 4-aryl substituted 5-alkoxycarbonyl-6-methyl-3,4-dihydropyridones under microwave irradiation. *Tetrahedron Letters*. 2003;**44**:3709-3712
- [41] Sharma SD, Gogoi P, Konwar D. A highly efficient and green method for the synthesis of 3,4-dihydropyrimidine-2-ones and 1,5-benzodiazepines catalysed by dodecyl sulfonic acid in water. *Green Chemistry*. 2009;**9**:153-157
- [42] Lewandowski K, Murer P, Svec F, Frechet JM. A combinational approach to recognition of chirality: Preparation of highly enantioselective aryl-dihydropyrimidine selectors for chiral HPLC. *Journal of combinational Chemistry*. 1999;**1**(1):105-112
- [43] Uhm YR. Magnetic properties and application of catalysts in Biginelli reaction for the Ni and Ni@C synthesized by Levitational gas condensation (LGC). *Journal of the Korean magnetism Society*. 2017;**27**(3):1-5
- [44] Metelitzka DI, Naumchik IV, Karasyova EI, Plozov GI, Shadyro OI. Inhibition of peroxidase-catalyzed oxidation of aromatic amines by substituted phenols. *Applied Biochemistry and Microbiology*. 2003;**39**(4):352-362
- [45] Mercier C, Chabardes P. Organometallic chemistry in industrial vitamin a and E synthesis. *Pure and Applied Chemistry*. 1994;**66**(7):1508-1518
- [46] Chen L, Tang R, Li Z, Liang S. An efficient and mild oxidation of α -isophorone catalysed by N-hydroxyphthalimide and copper chloride. *Bulletine Chemical Society*. 2012;**33**(2):459-463
- [47] Yermakov AY, Feduschak TA, Uimin MA, Mysik AA, Gaviko VS, Chupakin ON, Shishmakov AB, Kharchuk VG, Petrov LA, kotov YA, Vosmerikov AV, Korolyov AV. Reactivity of nanocrystalline copper oxide and its modification under magnetic field. *Solid State Ionics*. 2004;**172**:317-323
- [48] Muthaikumaran S, Gopalakrishnan R. Structural, FTIR and photoluminescence studies of Cu doped ZnO nanopowders by co-precipitation method. *Optical Materials*. 2012;**34**:1946-1953
- [49] Mohan R, Krishnamoorthy K, Kim S-J. Enhanced photocatalytic activity of Cu-doped ZnO nanorods. *Solid State Communications*. 2012;**152**(5):375-380

- [50] Han BS, Uhm YR, Kim GM, Rhee CK. Novel synthesis of nanorod ZnO and Fe-doped ZnO by the hydrolysis of metal powders. *Journal of Nanoscience and Nanotechnology*. 2007;**7**(11):4158-4160
- [51] Han BS, Uhm YR, Rhee CK. Synthesis for nanoflower and rod of ZnO by a surfactant free and low temperature method. *Surface Review and Letters*. 2010;**17**(2):173-176
- [52] Akcay H, Oguz A, Karapire C. Study of heavy metal pollution and speciation in Buyak Menderes and Gediz river sediments. *Water Research*. 2003;**37**:813-822
- [53] Jadwiga O. The determination of Zn, cd, Pb and cu in soil extracts by anodic stripping voltammetry. *Water, Air, and Soil Pollution*. 1989;**45**:43-48
- [54] Selehattin Y, Sultan Y, Gulsen S, Murat S. Direct determination of Zn heavy metal in tap water of Canakkale (TURKEY) by anodic stripping voltammetry technique. *International Journal of Electrochemistry and Science*. 2009;**4**:288-294
- [55] Raj J, Raina A, Mohineesh, Dogr TD. Direct Determination of Zinc, Cadmium, Lead, Copper Metal in Tap Water of Delhi (India) by Anodic Stripping Voltammetry Technique. In: *E3S Web of Conference*. Rome, India: EDP Sciences; April 2013. 09009. pp. 1-4
- [56] Novotry K, Turzikova A, Komarek J. Speciation of copper, lead and cadmium in aquatic systems by circulating dialysis combined with flame AAS. *Fresenius Journal of Analytical Chemistry*. 2000;**366**:209-212
- [57] Morales MG, Marin MRP, Blazquez LC, Pinilla-Gil E. Applicability of the bismuth bulk rotating disk electrode for heavy metal monitoring in undisturbed environmental and biological samples: Determination of Zn(II) in rainwater, tap water, and urine. *Analytical Methods*. 2014;**6**:8668-8674
- [58] Granado Rico MA, Olivares Martin M, Pinilla-Gil E. Modification of carbon screen-printed electrodes by adsorption of chemically synthesized bi nanoparticles for the voltammetric stripping detection of Zn(II), cd(II), and Pb (II). *Talanta*. 2009;**80**(2):631-635
- [59] Lee G-J, Kim CK, Lee MK, Rhee CK. Reliability evaluation of nano bi/silver paste sensor electrode for detecting trace metals. *Journal of Nanoscience and Nanotechnology*. 2012;**12**(7):5673-5677
- [60] Lee G-J, Kim C-K, Lee MK, Rhee CK. A study on optimization of Nano-sized bismuth binding technology using a Nafion solution. *Journal of the Korean Physical Society*. 2010;**57**(6):1667-1671
- [61] Lee HM, Lee G-J, Uhm YR, Lee HJ, Lee MK, Rhee CK. Synthesis of nanocrystalline bismuth and its application to the detection of trace metals. *Journal of Nanoscience and Nanotechnology*. 2010;**10**(1):309-313
- [62] Cesarino I, Gouveia-Caridade C, Pauliukaite P, Cavalheiro ETG. Characterization and application of bismuth film modified graphite-polyurethane composite electrodes. *Electroanalysis*. 2010;**22**(13):1437-1445

- [63] Marinkovic V, Agbaba D, Vladimirov S, Stankovic S. Simultaneous HPLC determination of nitrendipine and impurities of the process of synthesis. *Journal of Pharmaceutical and Biomedical Analysis*. 2001;**24**:993-998
- [64] Oliver Kappe C. Recent advances in the Biginelli Dihydropyrimidine synthesis new tricks from an old dog. *Accounts of Chemical Research*. 2000;**33**(12):879-888
- [65] Atwal KS, Rovnyak, O'Reilly GC, Schwartz. Synthesis of selectivity functionalized 2-Hetero-1,4-dihydropyrimidines. *Journal of Organic Chemistry*. 1989;**54**:5898-5907

IntechOpen